

# GAMMA-DEUTERON SCATTERING

S.R. BEANE

*Department of Physics, University of Maryland,  
College Park, MD 20742-4111  
E-mail: sbeane@physics.umd.edu*

We discuss a recent computation of Compton scattering on the deuteron at photon energies of order the pion mass. An interaction kernel is computed in baryon chiral perturbation theory and sewn to phenomenological deuteron wave functions. As an appetizer, we consider a computation of the pion-deuteron scattering length using this method.

## 1 Introduction

Precise calculations of hadron processes are possible only where a small dimensionless expansion parameter is identified. This is the main motivation behind the ongoing intense effort to develop a perturbative theory of nuclear interactions<sup>1</sup>. The dimensionless parameters relevant to low energy QCD and therefore to nuclear physics consist of ratios of external momenta to various characteristic energy scales, like the nucleon mass. Effective field theory is the technology which develops a hierarchy of scales into a perturbative expansion of physical observables. In a system with broken symmetries this technology is especially powerful. When a continuous symmetry is spontaneously broken there are massless Goldstone modes which dominate the low-energy dynamics and couple only derivatively. Hence at energies small relative to the characteristic symmetry breaking scale, the interactions of the Goldstone bosons can be ordered in an effective Lagrangian which is constrained by chiral symmetry and in which each operator contains a nonvanishing number of derivatives acting on the pion fields. Observables computed from the effective Lagrangian are therefore power series in momenta, with the non-analyticities required by perturbative unitarity.

In this paper we describe several recent effective field theory calculations whose objective is to extract nucleon properties from nuclear scattering processes in a systematic way. We first discuss the paradigmatic problem of the pion-deuteron scattering length and its dependence on nucleon parameters. We then describe a recent calculation of Compton scattering on the deuteron at photon energies of order the pion mass. Here the ultimate objective is to learn about neutron polarizabilities from nuclear Compton scattering. The basic power-counting scheme is reviewed in Sec. 2. In Sec. 3 we discuss the problem of pion-deuteron scattering at threshold as a heuristic tool. Sec. 4 is

dedicated to Compton scattering on the deuteron. We conclude in Sec. 5.

## 2 Weinberg power-counting

At energies well below the chiral symmetry breaking scale,  $\Lambda_\chi \sim 4\pi f_\pi \sim M \sim m_\rho$ , the interactions of pions, photons and nucleons can be described systematically using an effective field theory. This effective field theory, known as chiral perturbation theory ( $\chi PT$ ), reflects the observed QCD pattern of symmetry breaking. In QCD the chiral  $SU(2)_L \times SU(2)_R$  symmetry is spontaneously broken. Here we are interested in processes where the typical momenta of all external particles is  $p \ll \Lambda_\chi$ , so we identify our expansion parameter as  $p/\Lambda_\chi$ . In QCD  $SU(2)_L \times SU(2)_R$  is softly broken by the small quark masses. This explicit breaking implies that the pion has a small mass in the low-energy theory. Since  $m_\pi/\Lambda_\chi$  is then also a small parameter, we have a dual expansion in  $p/\Lambda_\chi$  and  $m_\pi/\Lambda_\chi$ . We take  $Q$  to represent either a small momentum *or* a pion mass.

In few-nucleon systems, a complication arises in  $\chi PT$  due to the existence of shallow nuclear bound states and related infrared singularities in  $A$ -nucleon reducible Feynman diagrams evaluated in the static approximation<sup>2</sup>. The fundamental problem is that nuclear physics introduces a new mass scale, the nuclear binding energy, which is very small compared to a typical hadronic scale like  $\Lambda_\chi$ . One way to overcome this difficulty is to adopt a modified power-counting scheme in which  $\chi PT$  is used to calculate an effective potential which generally consists of all  $A$ -nucleon irreducible graphs. The  $S$ -matrix, which includes all reducible graphs as well, is then obtained through iteration by solving a Lippmann-Schwinger equation<sup>2</sup>. This version of nuclear effective theory is known as the Weinberg formulation. To date the Weinberg formulation can be carried through rigorously only using finite cutoff regularization<sup>3,4,5,6</sup>. This limitation has spawned an intense theoretical effort geared at formulating an effective field theory for low-lying bound states which is verifiably (analytically) consistent in the sense of renormalization<sup>1</sup>. One result of this effort is a new power-counting scheme in which all nonperturbative physics responsible for the presence of low-lying bound states arises from the iteration of a single operator in the effective theory, while all other effects, including all higher dimensional operators *and* pion exchange, are treated perturbatively<sup>7,8</sup>. This version of the effective theory is known as the Kaplan-Savage-Wise (KSW) formulation. This is relevant here because Compton scattering on the deuteron has been computed to next-to-leading order in the KSW formulation<sup>9</sup>. We will discuss this result and its relation to our calculation. A comprehensive and up-to-date review of nuclear applications of effective field theories can be

found in Ref. <sup>1</sup>.

In the interactions of the deuteron with pionic and electromagnetic probes, Weinberg power-counting is encoded in the following simple diagrammatic rules:

- A nucleon propagator contributes  $Q^{-1}$ ;
- A pion propagator contributes  $Q^{-2}$ ;
- Each derivative or power of the pion mass at a vertex contributes  $Q$ . Therefore, an operator insertion from the  $\pi$ -N Lagrangian with  $n$  derivatives or powers of  $m_\pi$ ,  $\mathcal{L}_{\pi N}^{(n)}$ , contributes  $Q^n$ ;
- Each loop integral contributes  $Q^4$ ;
- Each deuteron wavefunction,  $\Delta$  or  $\nabla$ , contributes  $Q^{-\frac{1}{2}}$ .

It should be noted that typical nucleon momenta inside the deuteron are small—on the order of  $\sqrt{MB}$  or  $m_\pi$ , with  $B$  the deuteron binding energy—and consequently, *a priori* we expect no convergence problems in the  $\chi PT$  expansion of any low-momentum electromagnetic or pionic probe of the deuteron. Although in principle we could use wavefunctions computed in  $\chi PT$ , we will consider wavefunctions generated using modern nucleon-nucleon potentials. Generally we find that any wavefunction with the correct binding energy gives equivalent results to within the theoretical error expected from neglected higher orders in the chiral expansion. Presumably we are insensitive to short distance components of the wavefunction because we are working at low energies and the deuteron is a large object.

Weinberg power-counting has led to fruitful computation of many pionic and photonic probes of the two-nucleon system <sup>1</sup>, including the pion-deuteron scattering length <sup>10,11</sup>, neutral pion photoproduction on the deuteron at threshold <sup>12</sup>, Compton scattering on the deuteron <sup>13</sup>, as well as  $pn$  radiative capture <sup>14</sup> and the solar burning process  $pp \rightarrow de^+\nu$  <sup>15</sup>.

### 3 Appetizer: threshold $\pi$ -deuteron scattering

Effective field theory relates scattering processes involving a single nucleon to nuclear scattering processes. For instance, one can relate  $\pi$ -N scattering to  $\pi$ -nucleus scattering <sup>10,11</sup>. The non-perturbative effects responsible for nuclear binding are accounted for using phenomenological nuclear wavefunctions, as noted above. One can compute matrix elements using a variety of wavefunctions in order to ascertain the theoretical error induced by the off-shell behavior of different wavefunctions.

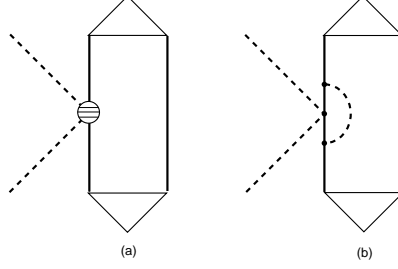


Figure 1: Contributions to the  $\pi$ -deuteron scattering length at order  $Q^2$  (a) and  $Q^3$  (b). The dots are vertices from  $\mathcal{L}_{\pi N}^{(1)}$  and the sliced blob is from  $\mathcal{L}_{\pi N}^{(2)}$ . All topologies are not shown.

To  $O(Q^3)$  in  $\chi PT$  the  $\pi$ -deuteron scattering length can be written as<sup>10</sup>

$$a_{\pi d} = \frac{(1 + \mu)}{(1 + \mu/2)}(a_{\pi n} + a_{\pi p}) + a^{(2a)} + a^{(2b,2c)}, \quad (1)$$

where  $\mu \equiv m_\pi/M$  is the ratio of the pion and the nucleon mass and the  $\pi$ -N scattering lengths have the decomposition

$$a_{\pi n} + a_{\pi p} = 2a^+ = a^{(1a)} + a^{(1b)} \quad (2)$$

where  $a^+$  is the isoscalar S-wave scattering length and the superscripts refer to the figures. The various diagrammatic contributions to  $a_{\pi d}$  are illustrated in Fig. 1 and Fig. 2. The leading contribution, Fig. 1(a), has three nucleon propagators ( $Q^{-3}$ ), a vertex from  $\mathcal{L}_{\pi N}^{(2)}$  ( $Q^2$ ), one loop ( $Q^4$ ) and two deuteron wavefunctions, ( $Q^{-1}$ ) giving a total of  $Q^{-3+2+4-1} = Q^2$ . Fig. 1(b) has five nucleon propagators ( $Q^{-5}$ ), one pion propagator ( $Q^{-2}$ ), three vertices from  $\mathcal{L}_{\pi N}^{(1)}$  ( $Q^3$ ), two loops ( $Q^8$ ) and two deuteron wavenfunctions, ( $Q^{-1}$ ) giving a total of  $Q^{-5-2+3+8-1} = Q^3$ . One can further verify that the graphs of Fig. 2 are  $O(Q^3)$ . Together, Figs. 1 and 2 are all that contribute at  $O(Q^3)$  at threshold.

The contributions to  $a_{\pi d}$  from the graphs of Fig. 2 are:

$$a^{(2a)} = -\frac{m_\pi^2}{32\pi^4 f_\pi^4 (1 + \mu/2)} \langle \frac{1}{\vec{q}^2} \rangle_{wf} \quad (3)$$

$$a^{(2b,2c)} = \frac{g_A^2 m_\pi^2}{128\pi^4 f_\pi^4 (1 + \mu/2)} \langle \frac{\vec{q} \cdot \vec{\sigma}_1 \vec{q} \cdot \vec{\sigma}_2}{(\vec{q}^2 + m_\pi^2)^2} \rangle_{wf} \quad (4)$$

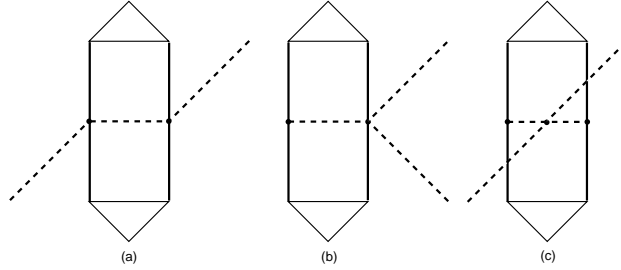


Figure 2: Two loop contributions (with an exchanged pion) to the  $\pi$ -deuteron scattering length at  $Q^3$ .

where  $\langle \vartheta \rangle_{wf}$  indicates that  $\vartheta$  is sandwiched between deuteron wavefunctions. These matrix elements have been evaluated using a cornucopia of wavefunctions; results are displayed in table 1. Clearly  $a^{(2a)}$  dominates. This is the result of the shorter range nature of  $a^{(2b,2c)}$ . It is important to stress that the dominant contribution from these graphs is quite independent of the wavefunction used. This implies that the  $\chi PT$  approach, which relies on the dominance of the pion-exchange, is useful in this context.

To  $O(Q^3)$  in  $\chi PT$ <sup>16</sup>:

$$4\pi(1+\mu)a^+ = \frac{m_\pi^2}{f_\pi^2} \left( -4c_1 + 2c_2 - \frac{g_A^2}{4M} + 2c_3 \right) + \frac{3g_A^2 m_\pi^3}{64\pi f_\pi^4}, \quad (5)$$

where the  $c_i$  are low-energy constants from  $\mathcal{L}_{\pi N}^{(2)a}$ . The sole undetermined parameter entering the  $O(Q^3)$  computation of  $a_{\pi d}$  is therefore a combination of  $c_1$ ,  $c_2$  and  $c_3$ :

$$\Delta \equiv -4c_1 + 2(c_2 + c_3). \quad (6)$$

There is recent experimental information about both the  $\pi$ -N and  $\pi$ -deuteron scattering lengths<sup>17,18</sup>. Since  $a^+$  involves constants that are not fixed by chiral symmetry we can use experimental information about  $\pi$ -deuteron scattering to predict  $a^+$ ; the recent Neuchatel-PSI-ETHZ (NPE) pionic deuterium measurement<sup>17</sup> gives

$$a_{\pi d} = -0.0259 \pm 0.0011 m_\pi^{-1}. \quad (7)$$

<sup>a</sup> It should be stressed that to this order there appear large cancellations between the individual terms<sup>16</sup> which lead one to suspect that a calculation at  $O(Q^4)$  should be performed to obtain a more precise prediction for this anomalously small observable.

Table 1: Contributions of Fig. 2 for various deuteron wavefunctions in units of  $m_\pi^{-1}$ . We use  $f_\pi = 92.4$  MeV,  $g_A = 1.32$  and  $m_{\pi^+} = 139.6$  MeV.

$wf$	$a^{(2a)}$	$a^{(2b,2c)}$
Bonn <sup>19</sup>	-0.02021	-0.0005754
ANL-V18 <sup>20</sup>	-0.01960	-0.0007919
Reid-SC <sup>21</sup>	-0.01941	-0.0008499
SSC <sup>22</sup>	-0.01920	-0.0006987

For the contributions of Fig. 2 we take the average of the  $a^{(2a)}$  and  $a^{(2b,2c)}$  values in table 1:

$$a^{(2a+2b+2c)} = -0.0203 m_\pi^{-1}. \quad (8)$$

We then find from Eq. (1):

$$a^+ = -(2.6 \pm 0.5) \cdot 10^{-3} m_\pi^{-1}. \quad (9)$$

Note that although  $a^{(2b,2c)}$  is small, there is a strong cancellation between  $a^{(2a)}$  and  $a_{\pi d}$  which leads to a sensitivity to  $a^{(2b,2c)}$ . Our value for  $a^+$  is not consistent with the Karlsruhe-Helsinki value<sup>23</sup>,

$$a^+ = -(8.3 \pm 3.8) \cdot 10^{-3} m_\pi^{-1}, \quad (10)$$

or the new NPE value deduced from the strong interaction shifts in pionic hydrogen and deuterium, which is small and positive<sup>18</sup>

$$a^+ = (0...5) \cdot 10^{-3} m_\pi^{-1}. \quad (11)$$

The result Eq. (9) agrees, however, with the value obtained in the SM95 partial-wave analysis<sup>24</sup>,  $a^+ = -3.0 \cdot 10^{-3} m_\pi^{-1}$ .

Given the ambiguous experimental situation regarding  $a^+$ , it seems most profitable to turn our formula around and use the  $\pi$ -deuteron scattering data to constrain  $\Delta$ . We can write

$$\Delta = \frac{2\pi f_\pi^2}{m_\pi^2} (1 + \mu/2) \{a_{\pi d} - (a^{(2a)} + a^{(2b,2c)})\} + \frac{g_A^2}{4M} \left(1 - \frac{3Mm_\pi}{16\pi f_\pi^2}\right). \quad (12)$$

Using Eqs. (3), (4) and (7) we find

$$\Delta = -(0.08 \pm 0.02) \text{ GeV}^{-1}, \quad (13)$$

where we have taken into account the error in the determination of  $a_{\pi d}$ .

Table 2: Values of the LECs  $c_i$  in  $\text{GeV}^{-1}$  for  $i = 1, \dots, 3$ . Also given are the central values (cv) and the ranges for the  $c_i$  from resonance exchange. The \* denotes an input quantity.

$i$	$c_i$	$c_i^{\text{Res}}$ cv	$c_i^{\text{Res}}$ ranges
1	$-0.93 \pm 0.10$	$-0.9^*$	—
2	$3.34 \pm 0.20$	3.9	$2 \dots 4$
3	$-5.29 \pm 0.25$	$-5.3$	$-4.5 \dots -5.3$
$\Delta$	$-0.18 \pm 0.75$	0.8	$-3.0 \dots +2.6$

In table 2 we give values of the relevant  $c_i$  obtained from a realistic fit to low-energy pion-nucleon scattering data and subthreshold parameters<sup>25</sup>. Central values lead to  $\sigma(0) = 47.6 \text{ MeV}$  and  $a^+ = -4.7 \cdot 10^{-3} m_\pi^{-1}$ . These values of the  $c_i$  give the conservative determination:

$$\Delta = -(0.18 \pm 0.75) \text{ GeV}^{-1}. \quad (14)$$

Also shown in table 2 are values of the  $c_i$  deduced from resonance saturation. It is worth mentioning that an independent fit to pion-nucleon scattering including also low-energy constants related to dimension three operators finds results consistent with the fit values of table 2<sup>26</sup>.

To summarize, we have shown that recent precise data on the  $\pi$ -deuteron scattering length can be used to constrain a combination of dimension two low-energy constants of the pion-nucleon chiral Lagrangian. This constraint can be improved by going to  $O(Q^4)$  in the chiral expansion. Thus this simple calculation provides an example of how using effective field theory one can extract nucleon properties from a nuclear process in a systematic way.

## 4 Entrée: $\gamma$ -deuteron scattering

### 4.1 Motivation

Nucleon Compton scattering has been studied in  $\chi PT$  in Ref.<sup>27</sup>, where the following results for the polarizabilities were obtained to order  $Q^3$ :

$$\begin{aligned} \alpha_p = \alpha_n &= \frac{5e^2 g_A^2}{384\pi^2 f_\pi^2 m_\pi} = 12.2 \times 10^{-4} \text{ fm}^3; \\ \beta_p = \beta_n &= \frac{e^2 g_A^2}{768\pi^2 f_\pi^2 m_\pi} = 1.2 \times 10^{-4} \text{ fm}^3. \end{aligned} \quad (15)$$

Here we have used  $g_A = 1.26$  for the axial coupling of the nucleon, and  $f_\pi = 93 \text{ MeV}$  as the pion decay constant. Note that the polarizabilities are *predictions*

of  $\chi PT$  at this order. The  $O(Q^3)$   $\chi PT$  predictions diverge in the chiral limit because they arise from pion loop effects. In less precise language, the power-counting of  $\chi PT$  implies that polarizabilities are dominated by the dynamics of the long-ranged pion cloud surrounding the nucleon, rather than by short-range dynamics. The polarizabilities should thus provide a sensitive test of chiral dynamics. At the next order in the chiral expansion,  $Q^4$ , there are contributions to the polarizabilities from undetermined parameters which must be fixed independently<sup>28</sup>. These counterterms account for short-range contributions to the nucleon structure.

Recent experimental values for the proton polarizabilities are<sup>29</sup> <sup>b</sup>

$$\begin{aligned}\alpha_p + \beta_p &= 13.23 \pm 0.86^{+0.20}_{-0.49} \times 10^{-4} \text{ fm}^3, \\ \alpha_p - \beta_p &= 10.11 \pm 1.74^{+1.22}_{-0.86} \times 10^{-4} \text{ fm}^3,\end{aligned}\tag{16}$$

where the first error is a combined statistical and systematic error, and the second set of errors comes from the theoretical model employed. These values are in good agreement with the  $\chi PT$  predictions.

On the other hand, the neutron polarizabilities are difficult to obtain experimentally due to the absence of suitable neutron targets and so the corresponding  $\chi PT$  prediction is not well tested. One way to extract neutron polarizabilities is to consider Compton scattering on nuclear targets. Consider coherent photon scattering on the deuteron. The cross section in the forward direction naively goes as:

$$\left. \frac{d\sigma}{d\Omega} \right|_{\theta=0} \sim (f_{Th} - (\alpha_p + \alpha_n)\omega^2)^2.\tag{17}$$

The sum  $\alpha_p + \alpha_n$  may then be accessible via its interference with the dominant Thomson term for the proton,  $f_{Th}$ <sup>30</sup>. This means that with experimental knowledge of the proton polarizabilities it may be possible to extract those for the neutron. Coherent Compton scattering on a deuteron target has been measured at  $E_\gamma = 49$  and 69 MeV by the Illinois group<sup>31</sup>. An experiment with tagged photons in the energy range  $E_\gamma = 84.2 - 104.5$  MeV is under analysis at Saskatoon<sup>32</sup>, while data for  $E_\gamma$  of about 60 MeV is being analyzed at Lund<sup>33</sup>.

Clearly the amplitude for Compton scattering on the deuteron involves mechanisms other than Compton scattering on the individual constituent nucleons. Hence, extraction of nucleon polarizabilities requires a theoretical calculation of Compton scattering on the deuteron that is under control in the

---

<sup>b</sup>These are the result of a model-dependent fit to data from Compton scattering on the proton at several angles and at energies ranging from 33 to 309 MeV.



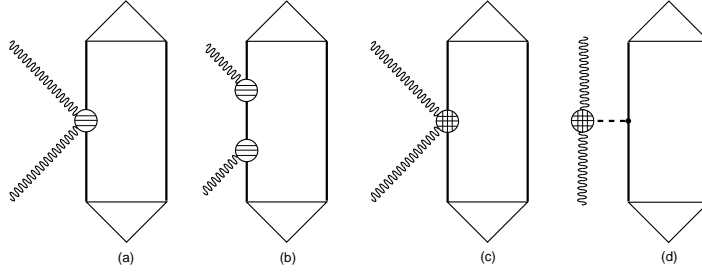


Figure 3: One loop graphs which contribute to Compton scattering on the deuteron at order  $Q^2$  (a) and at order  $Q^3$  (b-d) (in the Coulomb gauge). The sliced and diced blobs are from  $\mathcal{L}_{\pi N}^{(3)}$  (c) and  $\mathcal{L}_{\pi\gamma}^{(4)}$  (d). Crossed graphs are not shown.

sense that it accounts for *all* mechanisms to a given order in a systematic expansion in a small parameter. There exist a few calculations of this reaction in the framework of conventional potential models<sup>34,35,36</sup>. These calculations yield similar results if similar input is supplied, but typically mechanisms for nucleon polarizabilities and two-nucleon contributions are not treated consistently. We will see that  $\chi PT$  provides an alternative framework where this drawback can be eliminated.

In the remainder of this paper I will review a recent computation of Compton scattering on the deuteron for incoming photon energies of order 100 MeV in the Weinberg formulation. As in the computation of the pion-deuteron scattering length, baryon  $\chi PT$  is used to compute an irreducible scattering kernel to order  $Q^3$ , which is then sewn to external deuteron wavefunctions.

#### 4.2 Compton scattering to $O(Q^3)$

The Compton amplitude we wish to evaluate is (in the  $\gamma d$  center-of-mass frame):

$$T_{M'\lambda'M\lambda}^{\gamma d}(\vec{k}', \vec{k}) = \int \frac{d^3p}{(2\pi)^3} \psi_{M'} \left( \vec{p} + \frac{\vec{k} - \vec{k}'}{2} \right) T_{\gamma N_{\lambda'\lambda}}^{\gamma d \text{ c.m.}}(\vec{k}', \vec{k}) \psi_M(\vec{p}) \\ + \int \frac{d^3p \, d^3p'}{(2\pi)^6} \psi_{M'}(\vec{p}') T_{\gamma NN_{\lambda'\lambda}}^{2N}(\vec{k}', \vec{k}) \psi_M(\vec{p}) \quad (18)$$

where  $M$  ( $M'$ ) is the initial (final) deuteron spin state, and  $\lambda$  ( $\lambda'$ ) is the initial (final) photon polarization state, and  $\vec{k}$  ( $\vec{k}'$ ) the initial (final) photon three-

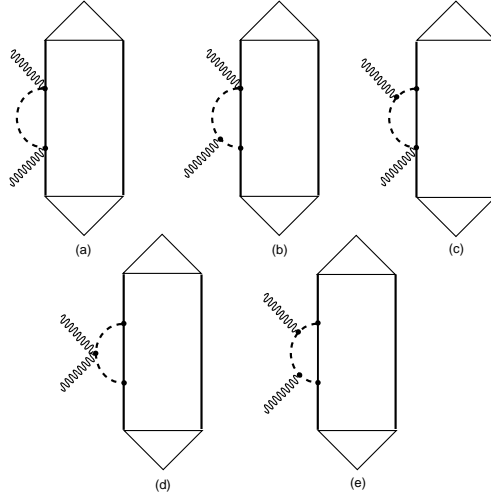


Figure 4: Two loop graphs which contribute to Compton scattering on the deuteron at order  $Q^3$ . Crossed graphs are not shown.

momentum, which are constrained to  $|\vec{k}| = |\vec{k}'| = \omega$ . The amplitude  $T_{\gamma N}^{\gamma d \text{ c.m.}}$  represents the graphs of figures 3 and 4 where the photon interacts with only one nucleon. Of course this amplitude must be evaluated in the  $\gamma d$  center-of-mass frame. The amplitude  $T_{\gamma NN}^{2N}$  represents the graphs of Fig. 5 where there is an exchanged pion between the two nucleons.

The leading contribution to Compton scattering on the deuteron is shown in Fig. 3(a). This graph has three nucleon propagators ( $Q^{-3}$ ), a vertex from the second order pion-nucleon Lagrangian ( $Q^2$ ), one loop ( $Q^4$ ) and two deuteron wavefunctions, ( $Q^{-1}$ ) giving a total of  $Q^{-3+2+4-1} = Q^2$ . This contribution is simply the Thomson term for scattering on the proton. At next order,  $O(Q^3)$ , there are several more one loop graphs Fig. 3(b,c,d) and two loop graphs without (Fig. 4) and with (Fig. 5) a pion exchanged between the nucleons. The full amplitudes are given in Ref. <sup>13</sup>.

For the wave function  $\psi$  we use the energy-independent Bonn OBEPQ wave function parameterization which is found in Ref. <sup>37</sup>. The photon-deuteron  $T$ -matrix (18) is then calculated and the laboratory differential cross section evaluated directly from it:

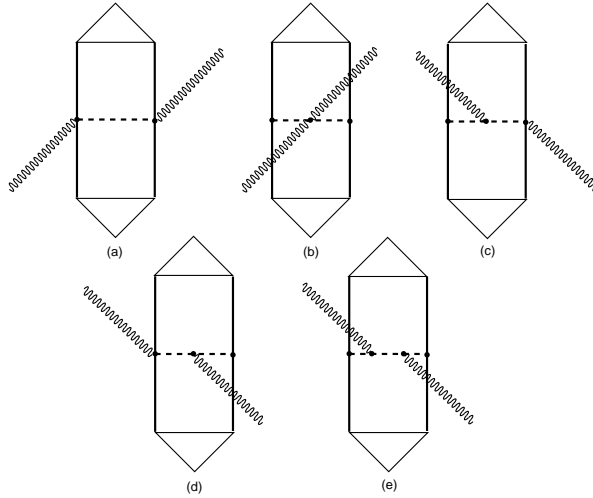


Figure 5: Two loop graphs which contribute to Compton scattering on the deuteron at order  $Q^3$ . Crossed graphs are not shown.

$$\frac{d\sigma}{d\Omega_L} = \frac{1}{16\pi^2} \left( \frac{E'_\gamma}{E_\gamma} \right)^2 \frac{1}{6} \sum_{M'\lambda'M\lambda} |T_{M'\lambda'M\lambda}^{\gamma d}|^2, \quad (19)$$

where  $E_\gamma$  is the initial photon energy in the laboratory frame and  $E'_\gamma$  is the final photon energy in the laboratory frame.

Convergence tests indicate that with the numbers of quadratures chosen the cross section evaluated in this fashion is numerically accurate at about the 1% level. Of course, this error does not include the theoretical error from uncertainties due to different deuteron wave functions<sup>c</sup>, and the effect of higher-order terms in  $\chi PT$ . The errors due to omitted higher orders in  $\chi PT$  will be discussed further below.

In figures 6, 7 and 8 we display our results at 49, 69, and 95 MeV. For comparison we have included the calculation at  $O(Q^2)$ , where the second contribution in Eq. (18) is zero, and the  $\gamma N$   $T$ -matrix in the single-scattering contribution is given by the Thomson term on a single nucleon. It is remarkable that to  $O(Q^3)$  no unknown counterterms appear. All contributions to the kernel are fixed in terms of known pion and nucleon parameters such as

<sup>c</sup>As discussed in detail in Ref. <sup>13</sup>, wavefunction errors are minimal and well understood.

$m_\pi$ ,  $g_A$ ,  $M$ , and  $f_\pi$ . Thus, to this order  $\chi PT$  makes *predictions* for Compton scattering.

The curves show that the correction from the  $O(Q^3)$  terms gets larger as  $\omega$  is increased, as was to be expected. Indeed, while at lower energies corrections are relatively small, in the 95 MeV results the correction to the differential cross section from the  $O(Q^3)$  terms is of order 50%, although the contribution of these terms to the *amplitude* is of roughly the size one would expect from the power-counting: about 25%. Nevertheless, it is clear, even from these results, that this calculation must be performed to  $O(Q^4)$  before conclusions can be drawn about polarizabilities from data at photon energies of order  $m_\pi$ . This is in accord with similar convergence properties for the analogous calculation for threshold pion photoproduction on the deuteron <sup>12</sup>.

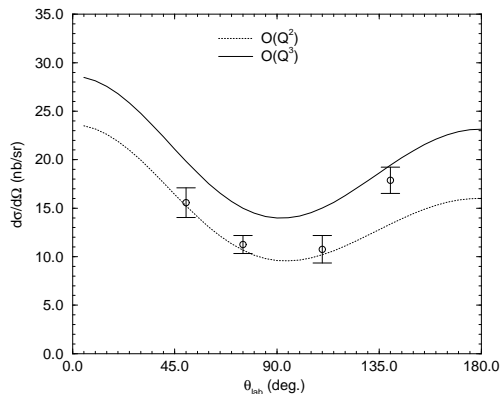


Figure 6: Results of the  $O(Q^2)$  (dotted line) and  $O(Q^3)$  (solid line) calculations at a photon laboratory energy of 49 MeV.

We have also shown the six Illinois data points at 49 and 69 MeV <sup>31</sup>. Statistical and systematic errors have been added in quadrature. It is quite remarkable how well the  $O(Q^2)$  calculation reproduces the 49 MeV data. However, it is clear that the agreement at forward angles is somewhat fortuitous, as there are significant  $O(Q^3)$  corrections. Meanwhile, the agreement of the  $O(Q^3)$  calculation with the 69 MeV data is very good, although only limited conclusions can be drawn, given that there are only two data points, each with sizeable error bars.

Our results are qualitatively not very different from other existing calcu-

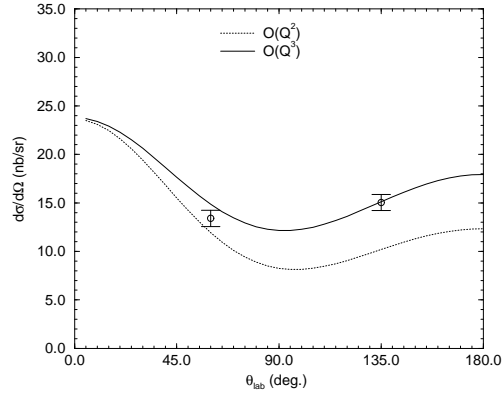


Figure 7: Results of the  $O(Q^2)$  (dotted line) and  $O(Q^3)$  (solid line) calculations at a photon laboratory energy of 69 MeV.

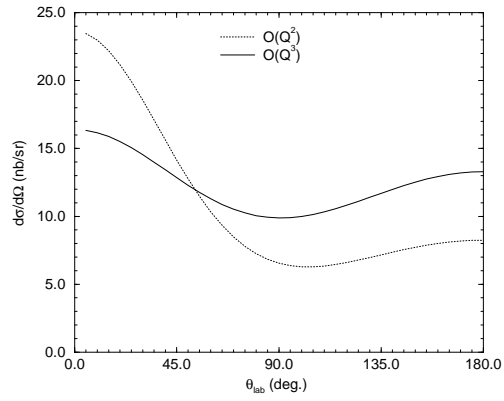


Figure 8: Results of the  $O(Q^2)$  (dotted line) and  $O(Q^3)$  (solid line) calculations at a photon laboratory energy of 95 MeV.

lations. At 49 and 69 MeV our  $O(Q^3)$  results are very close to those in Ref. <sup>34</sup> and a few nb/sr higher, especially at back angles, than those of Refs. <sup>35,36</sup> (which are similar at these energies). At 95 MeV our  $O(Q^3)$  result is close to that of Ref. <sup>35</sup>, higher by several nb/sr at back angles than Ref. <sup>36</sup>, and several nb/sr lower than the calculation with no polarizabilities of Ref. <sup>34</sup> <sup>d</sup>. Comparing to the calculations of deuteron Compton scattering in the KSW formulation of effective field theory<sup>9</sup>, we see that the result of Ref. <sup>9</sup> is significantly lower than those presented here at both 49 and 69 MeV. At 49 MeV the agreement of Ref. <sup>9</sup>'s calculation with the data is better than ours. We shall show in the next section that this is partly because 49 MeV is at the lower end of the domain of applicability of the Weinberg formulation. At 69 MeV our calculation does a slightly better job of reproducing the (two) data points available. The qualitative agreement among these calculations is a reflection of the similarities of mechanisms involved. Ours is however the only calculation to incorporate the full single-nucleon amplitude instead of its polarizability approximation. As shown in Fig. 9 our tendency to higher relative cross sections in the backward directions is at least in part due to this feature.

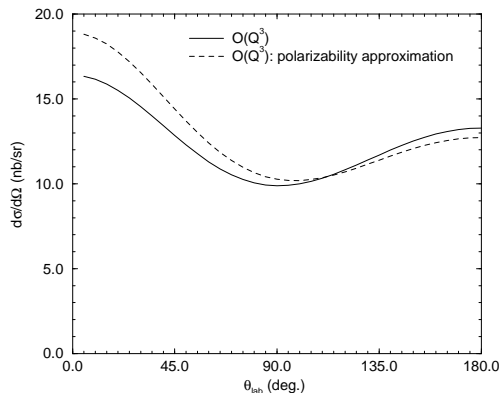


Figure 9: Unpolarized cross section for Compton scattering on the deuteron in deltaless  $\chi PT$  to  $O(Q^3)$  at 95 MeV. The polarizability approximation to the single-nucleon amplitude (dashed line) is to be compared with the full  $O(Q^3)$  calculation (solid line).

<sup>d</sup>At this energy Ref. <sup>34</sup> only presents results with  $\alpha_p + \alpha_n = \beta_p + \beta_n = 0$ , which in turn are considerably less forward peaked than the corresponding calculation of Ref. <sup>35</sup>.

### 4.3 Effective theories of Compton scattering

Although nominally the domain of validity of the Weinberg formulation extends well beyond the threshold for pion production, the power-counting fails at low energies well before the Thompson limit is reached. Consider the  $O(Q^4)$  contribution shown in Fig. 10. We can use this graph to illustrate the transition to the very-low energy regime  $Q \sim m_\pi^2/M$ . It is easy to see that this graph becomes comparable to the order  $Q^3$  graph of Fig. 5(a) when

$$\frac{|\vec{p}|^2}{\omega M} \sim 1. \quad (20)$$

Here  $\vec{p}$  is a typical nucleon momentum inside the deuteron and  $\omega$  is the photon energy. Since our power-counting is predicated on the assumption that all momenta are of order  $m_\pi$ , we find that power-counting is valid in the region

$$\frac{m_\pi^2}{M} \ll Q \ll \Lambda_\chi. \quad (21)$$

Therefore, in the region  $\omega \sim B$  the Weinberg power-counting is not valid, since the external probe momentum flowing through the nucleon lines is of order  $Q^2/M$ , rather than order  $Q$ . It is in this region that the Compton low-energy theorems are derived. Therefore our power-counting will not recover those low-energy theorems. Of course the upper bound on the validity of the effective theory should increase if the  $\Delta$ -resonance is included as a fundamental degree of freedom<sup>38</sup>.

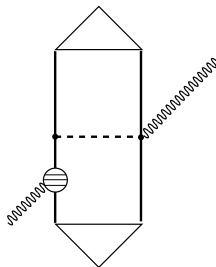


Figure 10: Interaction which contributes to Compton scattering on the deuteron at order  $Q^4$ . The sliced blob represents a  $1/M$  correction vertex from  $\mathcal{L}_{\pi N}^{(2)}$ .

In Ref.<sup>9</sup> Compton scattering on the deuteron was computed to the same order discussed here, one order beyond leading non-vanishing order but in the KSW formulation of two-nucleon effective field theory. An advantage of

KSW power-counting is that the effective field theory moves smoothly between  $Q < B$  and  $Q > B$ . KSW power-counting is valid for nucleon momenta  $Q < \Lambda_{NN} \sim 300$  MeV. Thus in the KSW formulation deuteron polarizabilities and Compton scattering up to energies  $\omega < \Lambda_{NN}^2/M \sim 90$  MeV can be discussed in the same framework. Here we are interested mostly in the region  $\omega \sim m_\pi$ , and so we regard ourselves as being firmly in the second regime. We stress that the value of  $\Lambda_{NN}$  is uncertain; it is conceivable that  $\Lambda_{NN} \sim 500$  MeV in which case the range of the KSW formulation would extend well beyond pion production threshold.

#### 4.4 Effects of higher order terms

In order to test the sensitivity of our calculation to higher-order effects we added a small piece of the  $O(Q^4)$  amplitude for Compton scattering off a single nucleon. Specifically, we have modified the Compton amplitudes so that the polarizabilities in the calculation are changed to

$$\alpha = \alpha^{(Q^3)} + \Delta\alpha, \quad \beta = \beta^{(Q^3)} + \Delta\beta, \quad (22)$$

where  $\alpha^{(Q^3)}$  and  $\beta^{(Q^3)}$  are the  $O(Q^3)$  values of Eq. (15). We emphasize that this effect represents only a part of what will appear in the single-nucleon scattering amplitude  $T_{\gamma N}$  at  $O(Q^4)$ . Furthermore, a number of additional mechanisms must be included in  $T_{\gamma NN}^{2N}$  in any  $O(Q^4)$  calculation of Compton scattering on the deuteron. Nevertheless, here we calculate the differential cross section with the modified polarizabilities in order to get a feel for the sensitivity of our result to the presence of such higher-order terms.

Two calculations were performed. In the first,  $\Delta\alpha$  and  $\Delta\beta$  were chosen so that the total polarizabilities (22) were equal to the “experimental” values<sup>e</sup>. The second calculation involved a more dramatic change in the polarizabilities:  $\Delta\alpha$  and  $\Delta\beta$  were chosen so that  $\alpha$  and  $\beta$  were equal to the  $O(Q^4)$  values of Ref. <sup>28</sup> where resonance-saturation has been used to estimate some of the  $O(Q^4)$   $\chi PT$  counterterms. In either case  $\Delta\alpha_p + \Delta\alpha_n$  is relatively small, while  $\Delta\beta_p + \Delta\beta_n$  is not large for “experimental” values, but is significant for the  $O(Q^4)$  values. The results of these two calculations for the two photon energies  $E_\gamma = 49$  MeV and  $E_\gamma = 95$  MeV are shown in Fig. 11 and Fig. 12.

In both cases we see that, just as one would expect, the cross section at 95 MeV is much more sensitive to these  $O(Q^4)$  terms than the cross section at 49 MeV. It is not surprising that the calculation with  $O(Q^4)$  polarizabilities exhibits a larger change than that with “experimental” values. Continually

---

<sup>e</sup>Here we use the proton experimental values and neutron “experimental” values (see Ref. <sup>13</sup> for details).



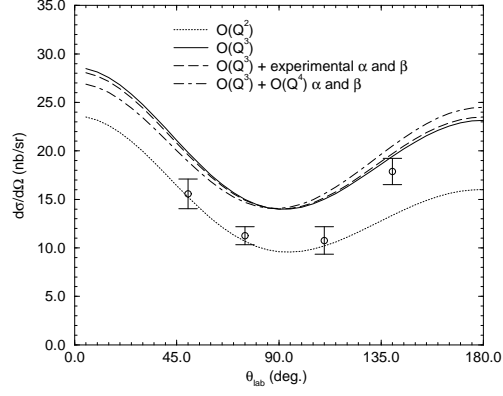


Figure 11: Results of calculations at 49 MeV using different values for the nucleon electromagnetic polarizabilities. The solid line is the result using the  $O(Q^3)$   $\chi PT$  value, the long-dashed line is the result using “experimental” polarizabilities, and the dot-dashed line represents a calculation with the  $O(Q^4)$  polarizabilities.

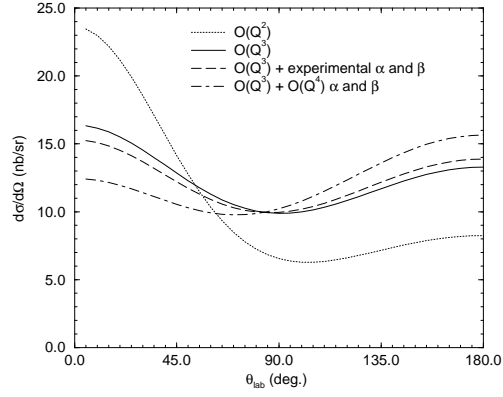


Figure 12: Results of calculations at 95 MeV using different values for the nucleon electromagnetic polarizabilities. Legend as in Fig. 11.

increasing  $\beta_p + \beta_n$  at approximately constant  $\alpha_p + \alpha_n$  decreases the cross section at forward angles and increases it at back angles. In fact, it seems that if  $\beta_p + \beta_n$  is sufficiently large then the character of the cross section at 95 MeV can change completely from forward peaked to backward peaked.

Significant change in the 95 MeV results presented here from those obtained at  $O(Q^3)$  mandates a cautious interpretation. At the same time that the cross section at 95 MeV is more sensitive to polarizabilities than at lower energies, it is also more sensitive to  $O(Q^4)$  corrections. In our view, a full  $O(Q^4)$  calculation in  $\chi PT$  is necessary if any attempt is to be made to extract the neutron polarizability from the Saskatoon data within this framework.

## 5 Dessert

Using effective field theory techniques, nucleon properties can be extracted systematically from experiments performed with nuclei. As a simple example, we have reviewed a  $\chi PT$  calculation which uses  $\pi$ -deuteron data to place constraints on low energy constants of the  $\pi$ -N chiral Lagrangian.

And, too, we have reviewed a recent computation of Compton scattering on the deuteron in  $\chi PT$ . We find reasonable agreement with the data at 49 MeV. At this energy  $O(Q^3)$  corrections are not large compared to the leading  $O(Q^2)$  result, and  $O(Q^4)$  terms seem to be even smaller. However, as anticipated, the effective theory appears to break down as the Thomson limit is approached. We find good agreement with the data at 69 MeV. At this energy the convergence appears to be good. This suggests that  $\chi PT$  at  $O(Q^3)$  is providing reasonable neutron and two-nucleon contributions. We find that the polarizability approximation should not be used in the calculation of the differential cross section at 95 MeV, since truncating the photon-nucleon amplitude at order  $\omega^2$  results in a significant change in the photon-deuteron differential cross section for forward angles. The wave function dependence is minor (on the order of 10% in the differential cross section). We make a prediction at 95 MeV which is, however, plagued by considerable uncertainties. Convergence is slow at this energy, as indicated by the relative size of both the full set of  $O(Q^3)$  corrections and a partial set of  $O(Q^4)$  corrections. The cross section tends to come out somewhat smaller than at lower energies, in particular in the backward directions, although the full  $O(Q^4)$  amplitude is likely to be somewhat bigger at back angles. It seems that a more stringent test of  $\chi PT$  at these energies—including aspects of neutron structure beyond the  $O(Q^3)$  “pion cloud” picture—will have to wait for a next-order calculation.

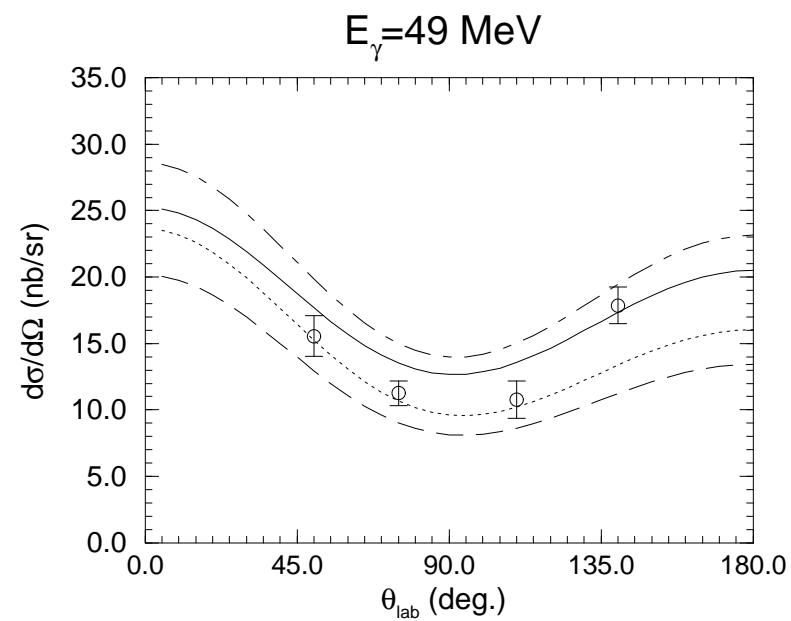
## Acknowledgments

I thank Veronique Bernard, Harry Lee, Mané Malheiro, Ulf Meißner, Dan Phillips and Ubi van Kolck for enjoyable collaborations, Dan and Ubi for comments on the MS and the INT for a great workshop. This research was supported by DOE grant DE-FG02-93ER-40762 (DOE/ER/40762-183, UMPP#99-112).

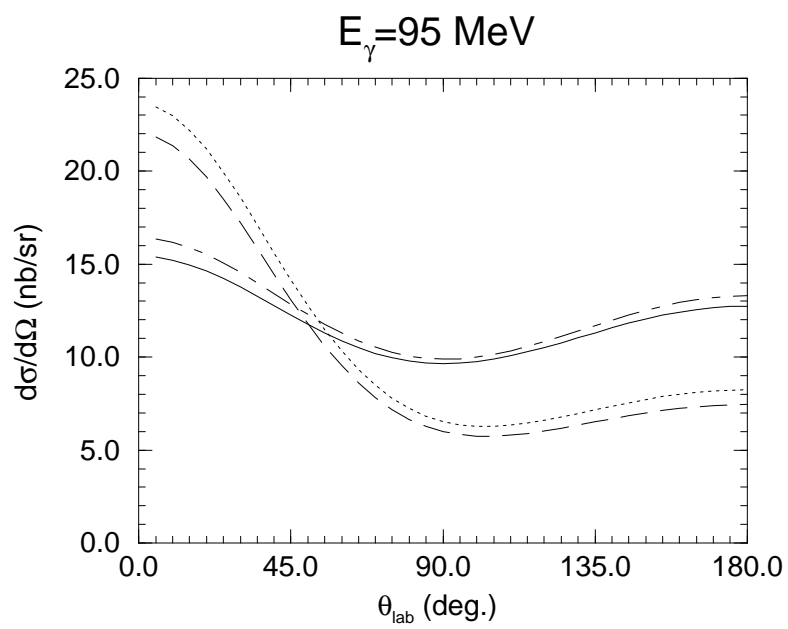
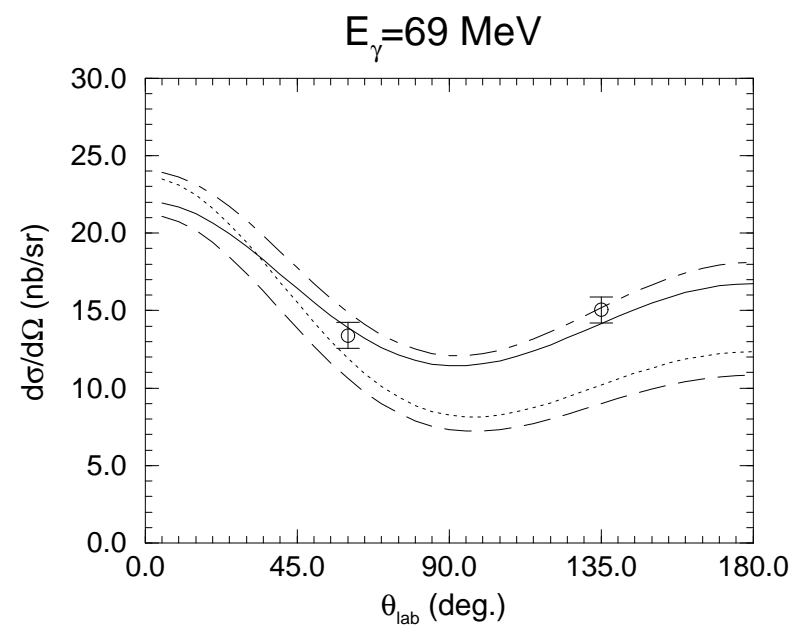
## References

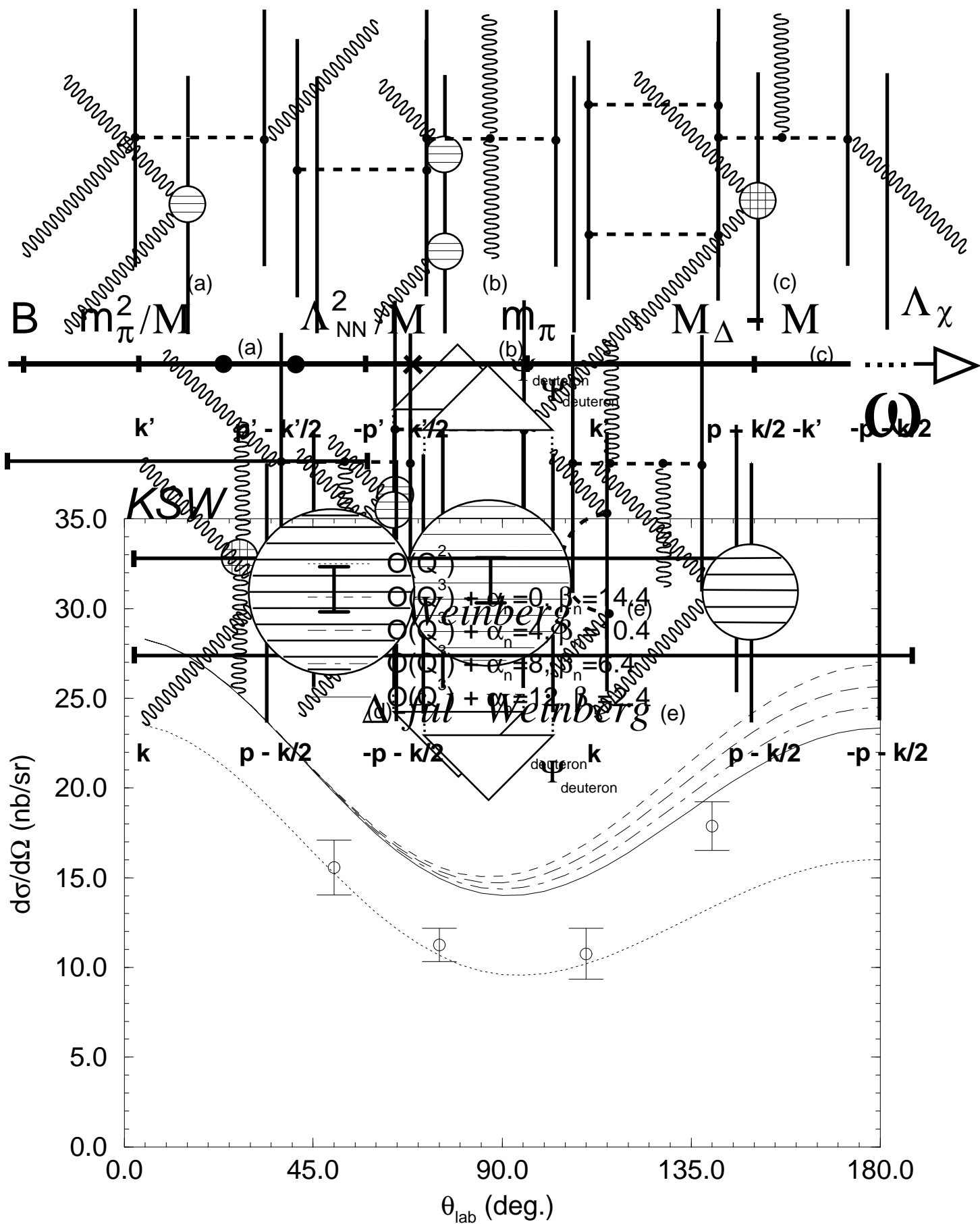
1. *Nuclear Physics with Effective Field Theory*, eds. R. Seki, U. van Kolck and M. J. Savage (World Scientific, 1998); U. van Kolck, [nucl-th/9902015](#).
2. S. Weinberg, *Phys. Lett. B* **251**, 288 (1990); *Nucl. Phys. B* **363**, 3 (1991).
3. C. Ordóñez and U. van Kolck, *Phys. Lett. B* **291**, 459 (1992); U. van Kolck, Ph. D. thesis, University of Texas (1993).
4. U. van Kolck, *Phys. Rev. C* **49**, 2932 (1994).
5. C. Ordóñez, L. Ray, and U. van Kolck, *Phys. Rev. Lett.* **72**, 1982 (1994); *Phys. Rev. C* **53**, 2086 (1996), [hep-ph/9511380](#).
6. G. P. Lepage, lectures given at the 9th Jorge Andre Swieca Summer School: Particles and Fields, Sao Paulo, Brazil, [nucl-th/9706029](#).
7. U. van Kolck, in *Mainz 1997, Chiral Dynamics: Theory and Experiment*, ed. A. Bernstein *et al.* (Springer-Verlag, 1998), [hep-ph/9711222](#); in Ref. <sup>1</sup>; *Nucl. Phys. A* **645**, 273 (1999), [nucl-th/9808007](#).
8. D. B. Kaplan, M. J. Savage, and M. B. Wise, *Phys. Lett. B* **424**, 390 (1998), [nucl-th/9801034](#); *Nucl. Phys. B* **534**, 329 (1998), [nucl-th/9802075](#).
9. J.-W. Chen, H. W. Griesshammer, M. J. Savage and R. P. Springer, [nucl-th/9806080](#); [nucl-th/9809023](#); J.-W. Chen, [nucl-th/9810021](#).
10. S. Weinberg, *Phys. Lett. B* **295**, 114 (1992).
11. S. R. Beane, V. Bernard, T.-S. H. Lee and Ulf-G. Meißner, *Phys. Rev. C* **57**, 424 (1998), [nucl-th/9708035](#).
12. S. R. Beane, C. Y. Lee, and U. van Kolck, *Phys. Rev. C* **52**, 2914 (1995), [nucl-th/9506017](#); S.R. Beane, V. Bernard, T.S.H. Lee, Ulf-G. Meißner and U. van Kolck, *Nucl. Phys. A* **618**, 381 (1997), [hep-ph/9702226](#); U. van Kolck, *these proceedings*.
13. S.R. Beane, M. Malheiro, D.R. Phillips and U. van Kolck, [nucl-th/9905023](#).
14. T.-S. Park, K. Kubodera, D-P. Min, and M. Rho, *Phys. Rev. C* **58**, 637 (1998), [hep-ph/9711463](#).

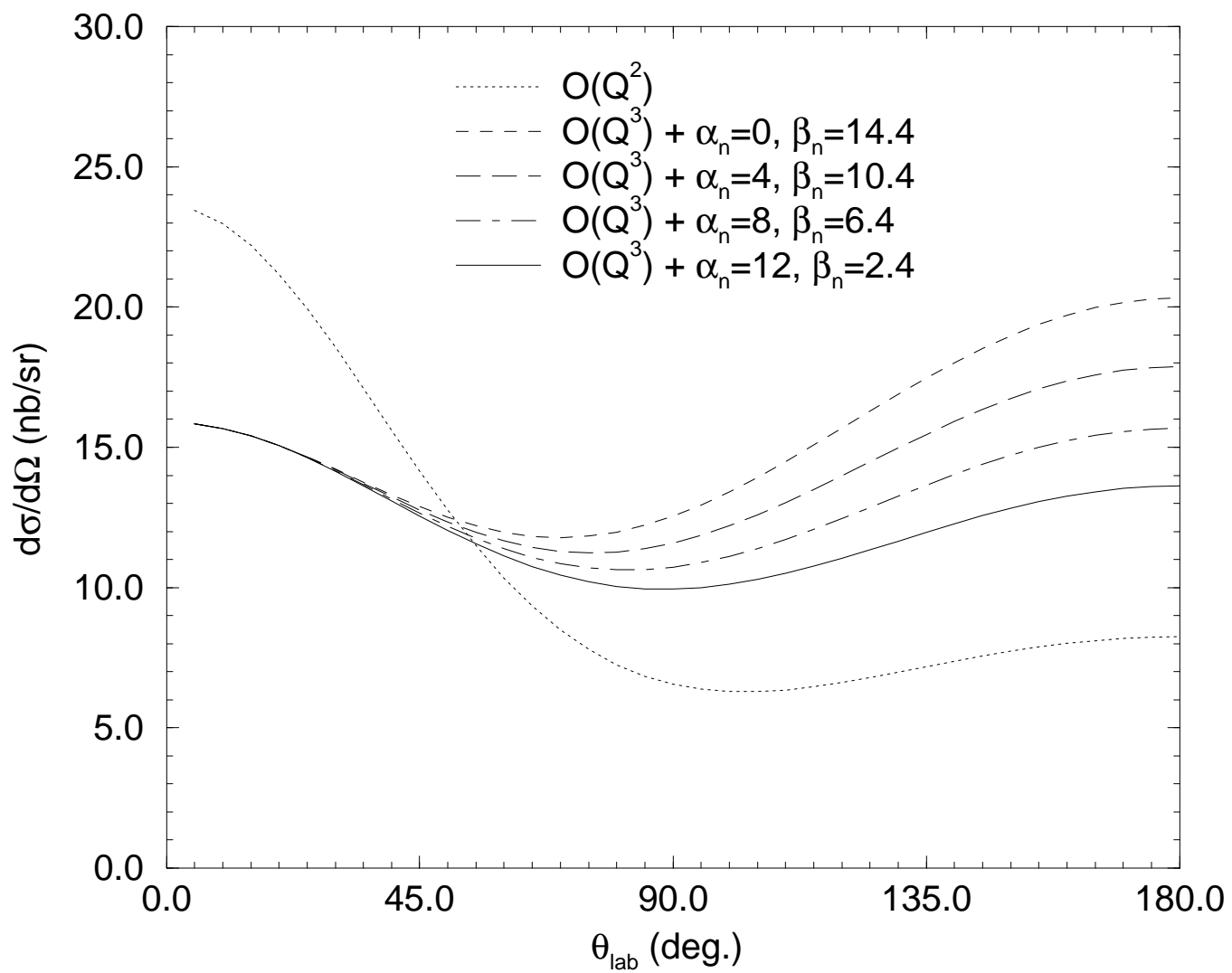
15. T.-S. Park, K. Kubodera, D-P. Min, and M. Rho, [astro-ph/9804144](#); *Nucl. Phys. A* **646**, 83 (1999), [nucl-th/9807054](#).
16. V. Bernard, N. Kaiser and Ulf-G. Meißner, *Phys. Lett. B* **309**, 421 (1993).
17. D. Chatellard et al., *Phys. Rev. Lett.* **74**, 4157 (1995); *Nucl. Phys. A* ,, i (n) print.
18. D. Sigg et al., *Phys. Rev. Lett.* **75**, 3245 (1995); *Nucl. Phys. A* **609**, 269 (1996); (E) A617, 526 (1997).
19. R. Machleidt, *ADV* **19**, 189 (1989).
20. R.B. Wiringa, V.G. Stoks and R. Schiavilla, *Phys. Rev. C* **51**, 38 (1995).
21. R.V. Reid, *Ann. Phys.* **50**, 411 (1968).
22. R. de Tournell and D.W. Sprung, *Nucl. Phys. A* **210**, 193 (1973).
23. R. Koch, *Nucl. Phys. A* **448**, 707 (1986).
24. R.A. Arndt et al., *Phys. Rev. C* **52**, 2120 (1995).
25. V. Bernard, N. Kaiser and Ulf-G. Meißner, *Nucl. Phys. A* **615**, 483 (1997).
26. M. Mojzis, [hep-ph/9704415](#), *Z.Phys.C*, in print.
27. V. Bernard, N. Kaiser, and Ulf-G. Meißner, *Phys. Rev. Lett.* **67**, 1515 (1991); *Nucl. Phys. B* **383**, 442 (1992); V. Bernard, N. Kaiser, J. Kambor, and Ulf-G. Meißner, *Nucl. Phys. B* **388**, 315 (1992).
28. V. Bernard, N. Kaiser, A. Schmidt, and Ulf-G. Meißner, *Phys. Lett. B* **319**, 315 (1993), [hep-ph/9309211](#); *Z. Phys. A* **348**, 317 (1994).
29. J. Tonnison, A. M. Sandorfi, S. Hoblit, and A. M. Nathan, *Phys. Rev. Lett.* **80**, 4382 (1998), [nucl-th/9801008](#).
30. D. Drechsel, *et al.*, in *Mainz 1997, Chiral Dynamics: Theory and Experiment*, ed. A. Bernstein *et al.*, (Springer-Verlag, 1998), p. 264, [nucl-th/9712013](#).
31. M. Lucas, Ph. D. thesis, University of Illinois, unpublished (1994).
32. D. Hornidge, private communication; G. Feldman, private communication.
33. M. Lunding, private communication.
34. T. Wilbois, P. Wilhelm, and H. Arenhövel, *Few-Body Sys. Suppl.* **9**, 263 (1995).
35. M. I. Levchuk and A. I. L'vov, [nucl-th/9809034](#), and references therein.
36. J. J. Karakowski and G. A. Miller, [nucl-th/9901018](#); J. J. Karakowski, Ph. D. thesis, University of Washington (1999), [nucl-th/9901011](#).
37. R. Machleidt, K. Holinde, and Ch. Elster, *Phys. Rep.* **149**, 1 (1987).
38. E. Jenkins and A. V. Manohar, *Phys. Lett. B* **255**, 558 (1991).

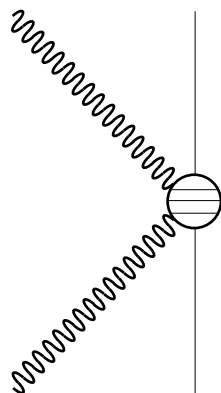


- $\cdots$   $O(Q^2)$
- $- - -$   $O(Q^2) + \text{NN contribution}$
- $- \cdot - \cdot -$   $O(Q^3)$
- $\text{—}$   $O(Q^3) + \text{NN contribution}$

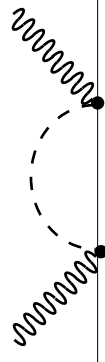






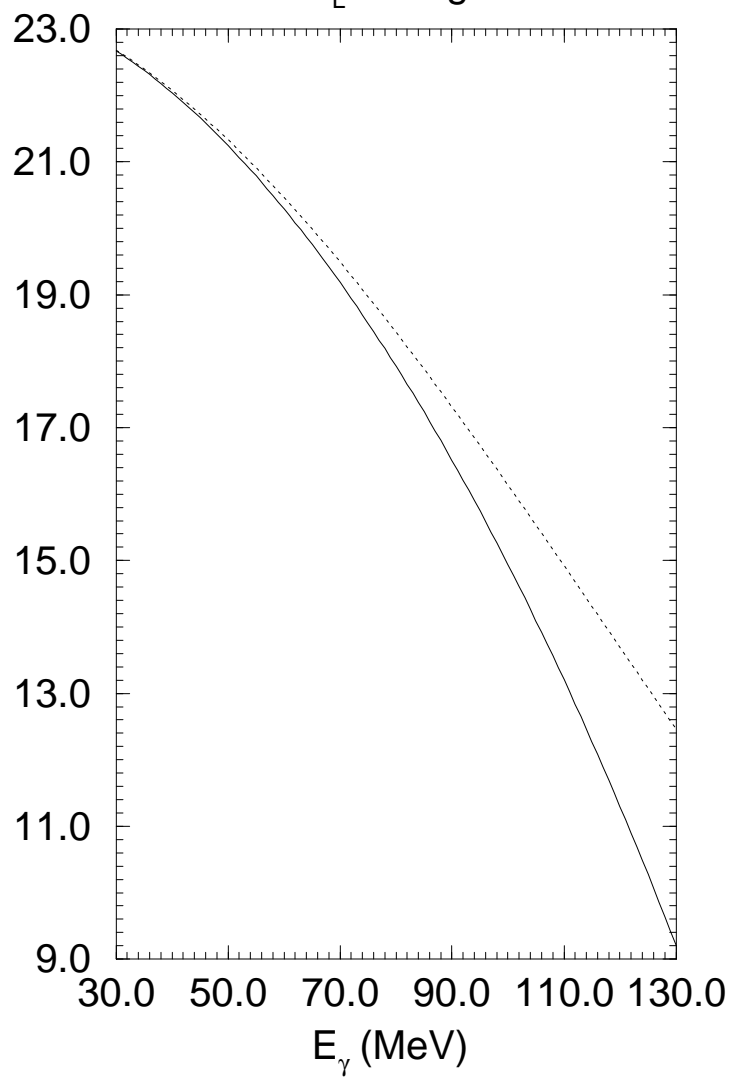


(a)



(b)

$\theta_L = 1$  deg.



$\theta_L = 180$  deg.

